Journal of ELECTRONIC MATERIALS, Vol. 48, No. 9, 2019
https://doi.org/10.1007/s11664-019-06983-4

Assessment of a Truck Localized Air Conditioning System with Thermoelectric Coolers

QIUSHI WAN,[1,2] CHUQI SU,[1,2] XIAOHONG YUAN,[1,2] LINLI TIAN,[1,2] ZUGUO SHEN,[1,2] and XUN LIU [1,2,3]

1.—Hubei Key Laboratory of Advanced Technology for Automotive Components, Wuhan University of Technology, 430070 Wuhan, China. 2.—Hubei Collaborative Innovation Center for Automotive Components Technology, Wuhan University of Technology, 430070 Wuhan, China. 3.—e-mail: liuxun@whut.edu.cn

In vehicles, the power consumption of the traditional air conditioning system used to cool an entire cabin reaches 3–4 kW. In general, there is only one driver in the vehicle, so adjusting the local thermal environment just around the driver can avoid much energy waste. A localized air conditioning system based on thermoelectric cooling (TEC) devices was constructed and assessed in an experimental study to analyze its working characteristics under practical operating conditions. The relationship between the refrigeration performance and the operating current of the devices was studied, and a bench test was carried out to evaluate the performance of the device and the accuracy of the simulation. A heavy-duty truck cab was selected for the application of the TEC system. The temperature distribution of the cab and the human body's surface was analyzed by the method of computational fluid dynamics to predict the performance of the whole system. The driver's thermal comfortwas analyzed based on equivalent temperature and thermal comfort deviation. Under given conditions, most body parts were in the comfort temperature range. The results indicated that the system can meet the thermal comfort requirements.

Key words: Thermoelectric cooling, localized cooling, air conditioning system, commercial vehicle

INTRODUCTION

In most cases, the power consumption of the traditional air conditioning (AC) system to cool the entire cabin of a vehicle will reach 3–4 kW on hot days in summer. However, statistical data show that there is always only one driver in the car, and therefore in the traditional AC system unnecessary cooling is often provided to the vacant seat areas. Therefore, this will cause a great waste of energy which also has a negative impact on the vehicle dynamic characteristics. What is more, the refrigerant of the AC system, mostly R134a (1,1,1,2-Tetrafluoroethane), has a global warming potential. Thus, it is worth studying automotive localized air conditioning systems which are used to control the local thermal environment just around the driver. Thermoelectric semiconductor refrigeration technology has many advantages such as no refrigerants, no moving parts, a compact structure, and precise temperature control.[1–7] Thus, thermoelectric cooling is very suitable for local thermal environment adjustment in the cabin. An automotive localized air conditioning system comprised of several thermoelectric cooling (TEC) devices can not only satisfy the driver's local thermal comfort but also save energy.[8–14]

When the Peltier effect was first proposed, researchers mainly focused on the refrigeration effect and applications.[15–17] Some studies were conducted on the application of TEC modules in the field of refrigeration or cooling systems. Abdul-Wahab[18] designed a portable solar thermoelectric refrigerator, and the experimental results showed

(Received October 2, 2018; accepted January 18, 2019; published online January 31, 2019)

that the temperature decreased from 27°C to 5°C in 44 min and the coefficient of performance (COP) value of that system was about 0.16. Min[19] established an experimental evaluation of a prototype thermoelectric refrigerator and found that, at an ambient temperature at 25°C, the COP value of this refrigerator was around 0.3–0.5 for a typical operating temperature of 5°C. Gillott[20] investigated thermoelectric cooling devices for mall-scale space cooling for which the COP could reach 0.46. Yilmazoglu[21] proposed a prototype heating and cooling device for a HVAC system based on thermoelectrics. The simulation and experiment research showed that the heating and cooling COP values of this kind of convective heat transfer HVAC unit varied between 2.5 and 5 and 0.4 and 1, respectively. Zhao and Tan[22] instructed a prototype thermoelectric system integrated with a phase-change-material (PCM) heat unit for space cooling. This system could reach an average cooling COP of 0.87 and a maximum cooling COP of 1.22, and the experiment revealed that using the PCM device yielded a 35.3% energy saving.

The research on local refrigeration or cooling systems has mainly focused on buildings and airplanes, while there are just a few applications in the automotive field. Kwon et al.[23] studied a local air conditioner that only adjusted the temperature of the driver's surroundings. Experiments had shown that this AC system could save 17–20% of electricity. Miranda et al.[24] demonstrated the feasibility of using semiconductor refrigeration technology in electric vehicle AC systems; the COP value of this air conditioning system could reach 1.7. Ghosh et al.[25] established the simulation model of a suburban utility vehicle with the local air conditioning system integrated into the cabin for computational fluid dynamics (CFD) simulation, and the influence of the local air conditioning on the cabin thermal environment was analyzed. Chen et al.[26] installed several semiconductor refrigeration devices in a cabin to form a local air conditioner to adjust the temperature of various parts of the driver. Wind tunnel test results showed that, when the driver was in a state of thermal comfort, this local air conditioning system yielded a 36.7% energy saving. Raut and Walke[27] developed a thermoelectric cooling system consisted of six TEC modules in a passenger car. The results indicated that the cabin temperature could be reduced by 4°C with a refrigeration power of 222 W.

However, only a few researchers (Chen et al.,[26] Raut and Walke[27]) have tried to combine the TEC unit with an automotive AC system. In their research, they ignored a significant matter which causes a large energy waste, which is that, in general, there is only one driver in the vehicle, so adjusting the local thermal environment just around the driver can avoid much energy waste. To the best of the authors' knowledge, there is no one using a localized air conditioning system with thermoelectric coolers. Moreover, all the research is based on passenger vehicles with no-one investigating commercial vehicles. In fact, commercial vehicles usually have a larger cabin space, which means that there will be more space for layouts and more energy saving potential.

To solve this problem, this study has focused on the application of local thermoelectric air conditioning systems in commercial vehicles. A local thermoelectric air conditioning system has two big energy advantages: it is localized, and can use TEC. This is the key to resolving the energy problem using a local air conditioning system with TEC units, which has not been studied by others.

The aim of the study was to develop a prototype local thermoelectric air conditioning system in a heavy-duty truck. Two designs of a thermoelectric cooling device with similar structures but different numbers of modules have been proposed and compared. Furthermore, the paper also establishes the simplified three-dimensional model of a truck containing a precise human model and studies the internal flow field distribution in the truck cabin and the temperature distribution of the human model's surface. The new local thermoelectric air conditioning system not only works with a low energy consumption but also meets the thermal comfort requirements of the driver.

STRUCTURE AND PRINCIPLE OF THERMOELECTRIC COOLING DEVICES

The thermoelectric cooling module consists of a cluster of thermocouples which are made of two different semiconducting thermo-elements. Based on the Peltier effect, when a voltage in the appropriate direction is applied through a connected junction, the thermocouples will generate a thermoelectric cooling effect.[22] Figure 1 shows the construction of the thermoelectric cooling device designed in this study. The device is made up of fins, TEC modules, clamping devices, insulation materials, fans, cooling water tanks and other auxiliary components. The internal structure of the cooling water tanks is also proposed. The fins are the cold-side heat exchangers. They are used to increase the heat transfer area of the air flow, thereby reducing the air temperature at the outlet, which will increase the cooling efficiency of the device. There are a total of 52 fins in the device, each fin being 94 mm long, 28 mm high and 1 mm wide with a gap of 1.5 mm between them. The hot sides of the TEC modules cling to the cooling water tanks to keep the temperature at a suitable level so that the cold sides which are the cold sources of the device can provide a more stable refrigeration power. Table I shows the characteristics of the TEC modules used in this study.

In the initial stages of this study, two structures were taken into consideration. As shown in Fig. 1, TEC1 has two modules and a cooling water tank,

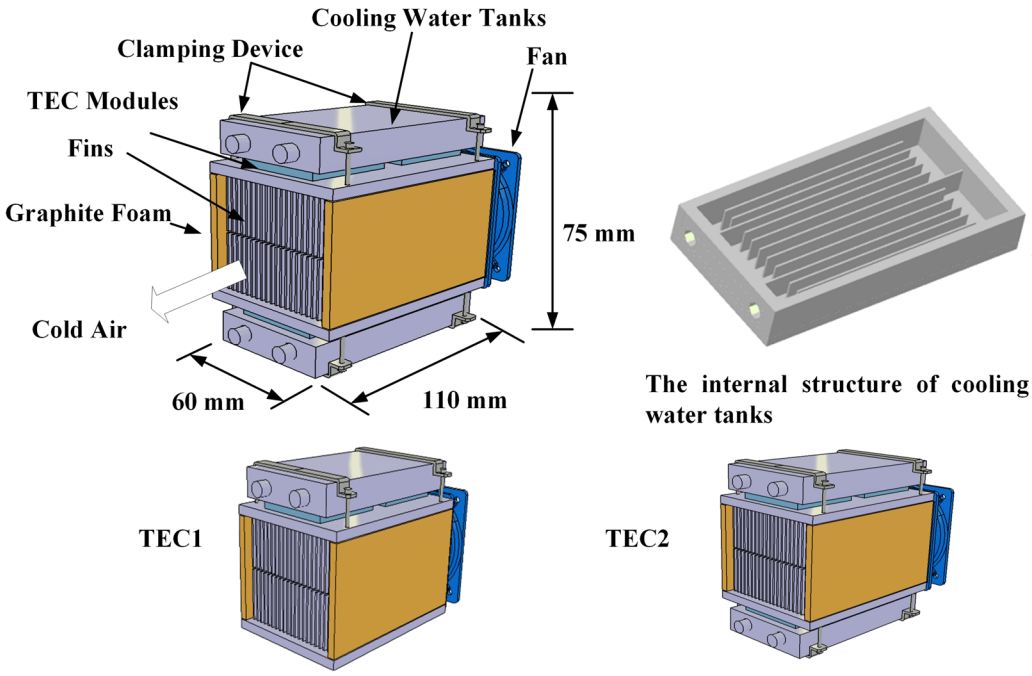

Fig. 1. Structure diagram of the two thermoelectric cooling devices.

Table I. Characteristics of the thermoelectric cooling module

Size	Internal resistance	Maximum temperature difference	Maximum refrigeration power	Rated voltage
40 × 40 × 3.7 mm	2.1–2.4Ω	67°C (Qc = 0°C)	50–60 W	12 V

and TEC2 has four modules and two cooling water tanks. The dimensions of the other components of the two devices are the same. This is intended to analyze the effect of the number of modules on the outlet air temperature and the efficiency of both devices.

THERMAL FIELD ANALYSIS

Simulation Set Up

Transient numerical simulations based on the finite element method have been carried out to analyze the performance of two thermoelectric cooling devices. The thickness of the insulating layer of the thermoelectric module is 0.75 mm and the material is alumina. The maximum flow rate of the fan is 48 cfm, with a maximum wind speed is 3 m/s. The specific parameters of the materials of these components are shown in Table II. The ambient temperature was assumed to be constant at 30°C. All the modules were connected in parallel with an operating current of 5 A for each. The flow of cooling water was set as 0.2 L/s and the inlet temperature was 25°C. The state of the device after 600 s of operation was simulated. Energy equations and an automatic algebraic turbulence model were selected.

Results and Discussion

In the simulation, the temperature distributions of the modules and other components, outlet temperature, cooling efficiency, and refrigeration power of the device have been investigated and analyzed. As mentioned above, TEC1 has two thermoelectric cooling modules while TEC2 has two layers of two modules each to give a total of four. Two modules of TEC2, which were on the same side, were selected to compare with two TEC1 modules. Figure 2 shows the temperature distributions of (a) cold sides, (b) hot sides, and (c) longitudinal sections of these modules.

As can be seen from Fig. 2a, the temperature of the cold side of the left module of TEC2 was from 10.2°C to 12.1°C, and the temperature of the right one was from 12.2°C to 14.3°C. The two modules which were in the same device had the same input current but the temperature of the cold side of the left module was lower, because the cooling water temperature increased. The temperature of the cold

Table II. Specific parameters of the materials of the components

Components	Material	Density (kg/m^3)	Thermal conductivity (W/m K)	Specific heat capacity (J/kg K)
Fins	Al 6061	2700	180	963
Cooling water tanks	Al 5052	2680	137	921
Insulation materials	Graphite foam	550	0.04	7000

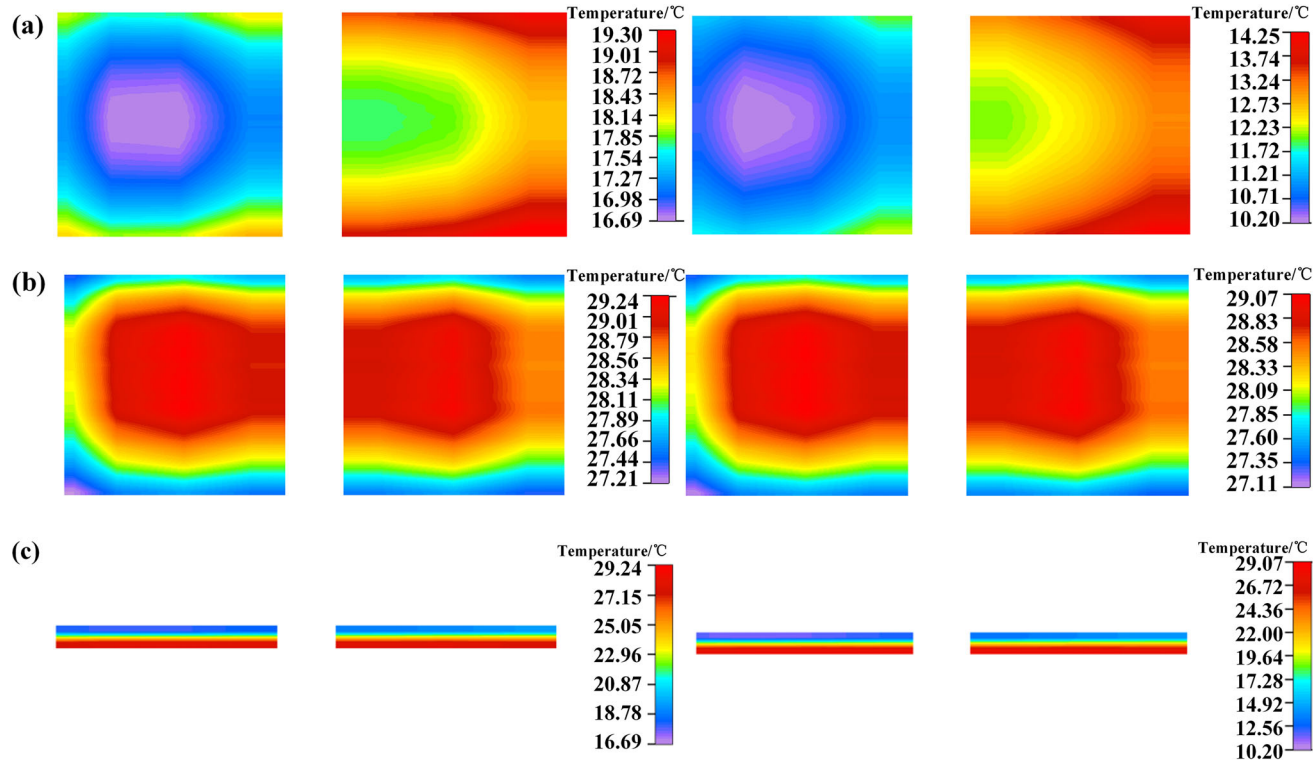

Fig. 2. Temperature distribution of two TEC of (a) cold sides, (b) hot sides and (c) longitudinal sections.

Table III. Simulation results of thermoelectric cooling modules

Device	Module number	Refrigeration power	Input power	Temp. difference	Max. temp. of hot side	Avg. temp. of cold side	COP (module)	COP (device)
TEC1	TEC1-1	37.17 W	41.78 W	10.31°C	29.24°C	17.93°C	0.89	0.89
	TEC1-2	37.4 W	42.03 W	11.43°C	29.28°C	17.61°C	0.89	
TEC2	TEC2-1	34.43 W	38.91 W	15.61°C	29.10°C	13.22°C	0.88	0.9
	TEC2-2	34.08 W	38.33 W	17.58°C	29.12°C	11.23°C	0.89	
	TEC2-3	34.52 W	38.83 W	15.45°C	29.45°C	14.06°C	0.89	
	TEC2-4	35.14 W	38.27 W	17.44°C	29.03°C	11.12°C	0.92	

side of the left side of the TEC1 was between 16.7°C and 18.1°C and that of the right side was between 18.2°C and 19.3°C, both of which were higher than that of the TEC2. As for the hot sides of these modules, which can be seen in Fig. 2b, the temperature distributions of TEC1 and TEC2 were similar. Other detail simulation results are presented in Table III. When the input current was 5 A, the total refrigeration power of the TEC1 was about 74.6 W, the input power was about 83.8 W, and the COP was 0.89. The total refrigeration power of the TEC2 was about 138.2 W, the input power was about

154.3 W, and the COP was 0.9. It can be concluded that, because of the different number of modules, the refrigeration power and input power of TEC1 were less than TEC2; however, the cooling efficiency of both devices was close.

The above simulation results were obtained with a working current of 5 A for each module. The total input power, refrigeration power, COP, and outlet temperature of the two devices with different working currents was also investigated, and the results are shown in Fig. 3. It can be seen that the variation of the parameters of these two devices was close. When the working current was less than 3 A, the COP was high but the refrigeration power was too low, and the cooling effect was not good enough. When the working current was more than 6 A, the outlet temperature and the refrigeration were close to stability. Although the cooling effect was better this time, the substantial increase of power consumption and the decrease of COP value will lead to energy waste. Obviously, the performances of the devices were not ideal under the above two conditions. Thus, for relatively preferable cooling performance and economy, the appropriate working current was from 3 A to 6 A.

Performance comparisons of the two devices at reasonable working currents was carried out and the results are shown in Table IV. It can be seen that, because of the two extra modules, the power consumption of TEC2 was about twice that of TEC1. However, more modules could also provide a lower air temperature and a wider outlet temperature range with more refrigeration power. The COP values were close, and the cooling efficiency of both devices was similar. The traditional automotive AC outlet temperature is from 12°C to 18°C. Therefore, the TEC1, which has two TEC modules, may not have enough cooling capacity, so selecting TEC2 to make up the automotive local air conditioning system is more appropriate under comprehensive consideration.

EXPERIMENTAL

A device has been built based on the TEC2 model. A bench test was carried out to evaluate the performance of the device and the accuracy of the simulation. The relationship between the input current, the input power and the air temperature were also studied through the experiments. Silicone grease was applied to the module surfaces to fill the gaps between the modules and the heat exchangers because of the surface roughness. Insulation boards were installed on both sides of the fins to reduce the loss of cooling load. Figure 4 shows the installation process of the thermoelectric cooling device.

Figure 5 presents the test bench developed in this study. The whole test bench includes the thermoelectric cooling device, data recorder, temperature sensors, cooling water pipes, water container, power supply with adjustable current and voltage, and the water pump. The device's four thermoelectric modules were connected in parallel. During the exper-

Table IV. Performance comparisons of the two devices at reasonable working currents

Parameters	TEC1	TEC2
Reasonable working currents	3–6 A	3–6 A
Input power	30–121 W	61–245 W
Refrigeration power	56–81 W	107–153 W
COP	0.67–1.88	0.63–1.75
Outlet temperature	21.2–23.9°C	13.8–18.6°C

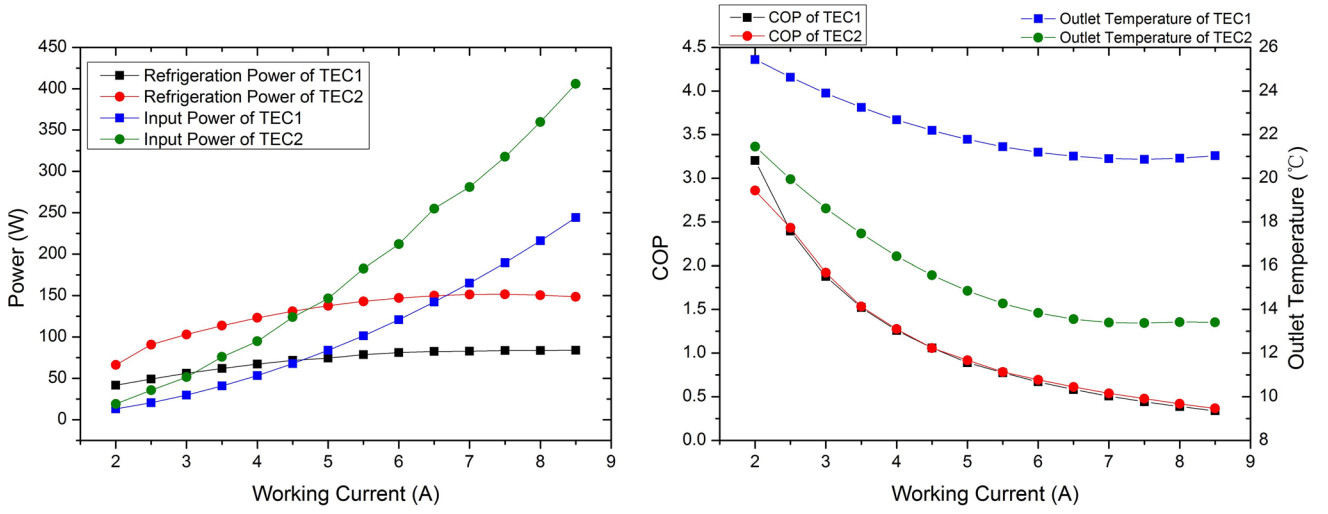

Fig. 3. Refrigeration performances of TECs with different working currents.

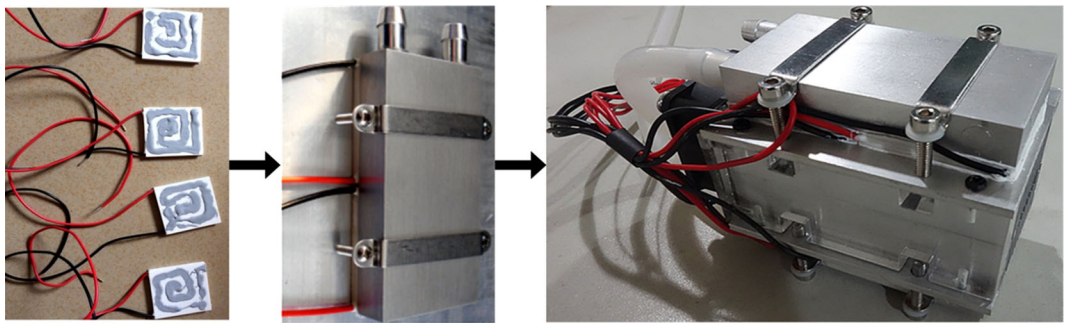

Fig. 4. Installation process of the thermoelectric cooling device.

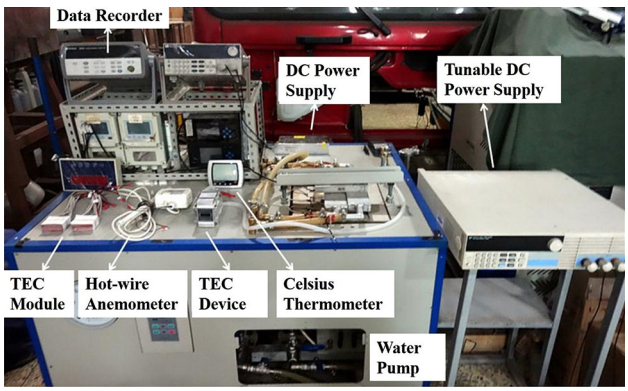

Fig. 5. Thermoelectric cooling device performance test bench.

iment, the operating current of each module was gradually increased from 2 A to 8.5 A. The total input power of the cooling device and the outlet temperature were recorded every 0.5 A. The experiment was repeated after 30 min, during which time the device temperature returned to room temperature.

The experimental results are shown in Fig. 6. The trends of the simulation and the test were close. The power consumption of the experiment was larger, which can be attributed to the conductor resistance loss. The lowest outlet temperature of the experiment was 15.4°C. The temperature of the test was about 2° higher than the simulation. Because, in the simulation, the module's electrical resistivity, Seebeck coefficient, and thermal conductivity were assumed to be constant, they did not vary with temperature. The thermal contact resistance between the modules and the heat exchangers was also ignored.

PERFORMANCE EVALUATION OF AUTOMOBILE LOCALIZED AIR CONDITIONING SYSTEM

A commercial vehicle, a heavy-duty truck cabin, was chosen for the application. It can also provide enough space for the arrangement of the devices. The automotive localized air conditioning system developed in this study is shown in Fig. 7. Six TEC devices were used for the localized cooling. One device was arranged above the driver's head, two devices were arranged in front of the shoulders, one device was on the back, and the remaining two were arranged near the feet. The CFD simulation was carried out to analyze the cabin's internal flow field and the body surface temperature field. The simulation results were used to predict and evaluate the performance of the system.

A three-dimensional model of the cabin and the human body was built, with some parts simplified to reduce the amount of computation. Table V shows the specific parameters of each component and relevant simulation boundary conditions. Some components were made of multiple layers of materials and the equivalent thermal resistance was used to obtain the thermal conductivity (Eq. 1).

$$\sum_{i=1}^{n} \frac{\delta_i}{\lambda} = \sum_{i=1}^{n} \frac{\delta_i}{\lambda_i} \tag{1}$$

where δ_i and λ_i represent the thickness and thermal conductivity of each layer of material, respectively, λ represents the equivalent thermal conductivity.

Except for TEC6 which was at the back, the outlet wind speed of the other five thermoelectric cooling devices was set as 3 m/s. The wind speed of TEC6 was 2 m/s. The outlet temperatures of the six devices were 18°C, 19°C, 19°C, 20°C, 20°C and 21°C, respectively. The RNG k–ε turbulence model was selected because of its high computational accuracy and strong adaptability. The external ambient temperature was set as 38°C to simulate the summer condition. Solar radiation was also taken into consideration, in order to make the simulation consistent with the real solar radiation situation, a site at Wuhan University of Technology (30°N, 114°E) was chosen, and the solar direct date was set at 12 am on July 20, 2017, which was a bright, sunny and cloudless day. The direction vector of the sun was (– 0.137, – 0.109, – 0.985). Table VI shows the relevant simulation boundary conditions.

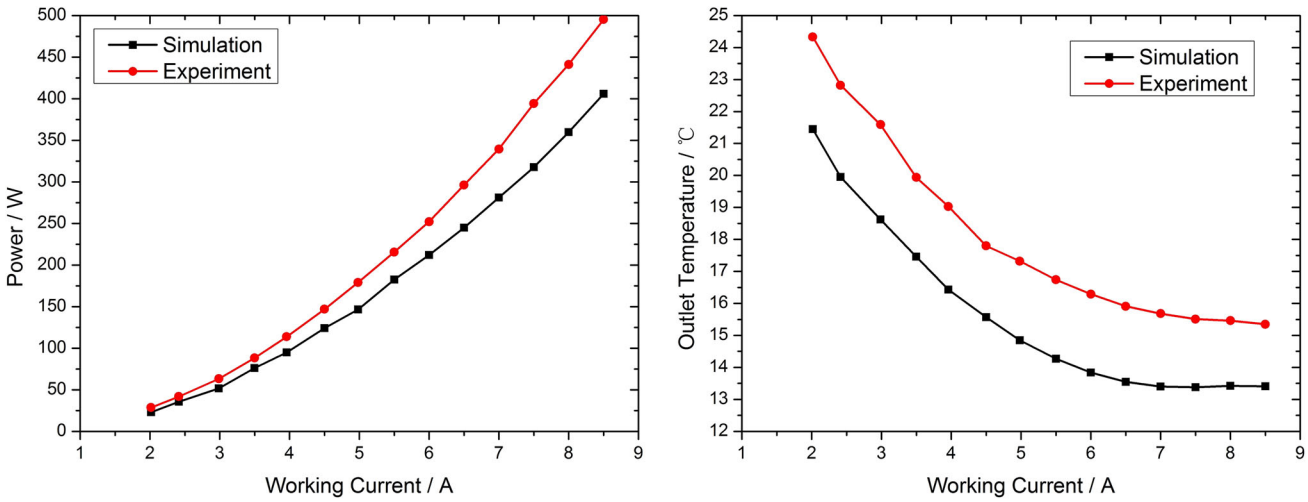

Fig. 6. Comparison of experimental and simulation results.

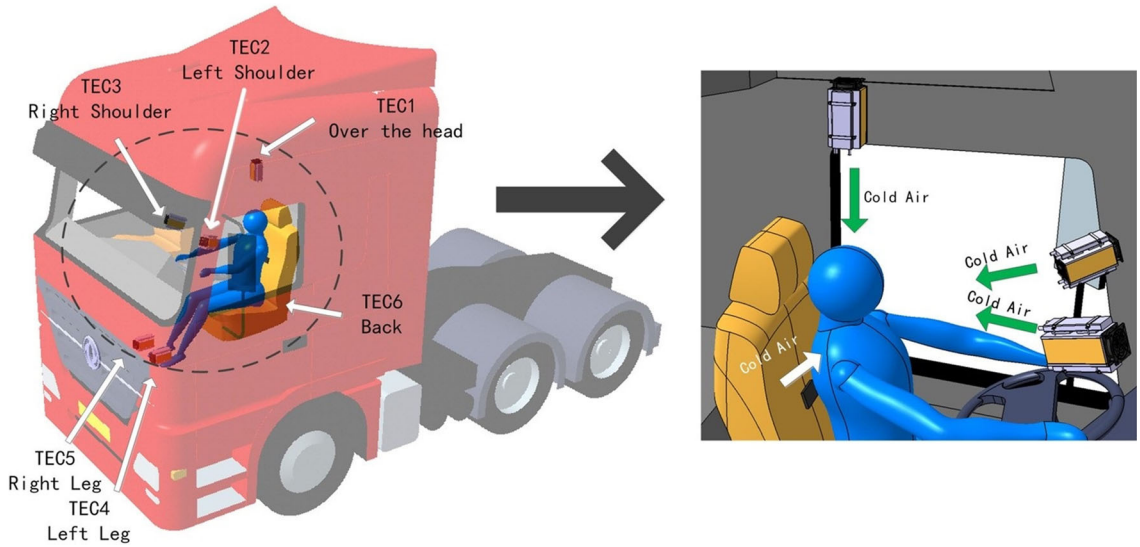

Fig. 7. Composition diagram of the automobile localized air conditioning system.

Figure 8 shows temperature maps of the cabin obtained by the CFD simulation. It can be seen from Fig. 8a that, because of the sun irradiation, the cabin surface temperature reached 46°C. A low temperature area was around the human body. Figure 9 presents the temperature map of the human body. The body surface temperature ranged from 25.7°C to 34.9°C. The upper part of the body had a lower temperature than the lower part. The temperature distributions of most parts of the human body were uniform.

Because the body surface temperature map cannot clearly reflect the effect of the cooling, the analysis of human thermal comfort is necessary. At present, there are two main methods to evaluate the thermal comfort of the human body, namely, the subjective evaluation method and the objective evaluation method. The subjective evaluation method allows participants to fill in a thermal comfort questionnaire to obtain the body's thermal comfort subjective feeling. Because the operation of this method is simple and convenient, the results are straightforward and it is a more common method of evaluation. However, there is much inaccuracy and ambiguity coming from the subjectivity and individual differences. In contrast, the objective evaluation method does not depend on subjective judgments. The reasonable evaluation indicators, combined with numerical simulation, can study the human thermal comfort

Table V. Physical parameters of cabin main components

Components	Surface thickness (mm)	Material	Density (kg/m^3)	Thermal conductivity (W/m K)	Specific heat capacity (J/kg K)	Convection heat transfer coefficient (W/m^2 K)	Absorptivity	Reflectivity	Transmissivity
Front windshield	5	Laminated glass	2529.6	0.91	754	6.38	0.40	0.10	0.5
Door windows	3.5	Tempered glass	2529.6	0.75	790	4.60	0.40	0.10	0.5
Body maintenance structure	8.6	Multilayer materials	8030	7.65	502.48	28.8	0.58	0.42	0.0
Floor	7.6	Multilayer materials	930	0.93	1480	4.68	0.58	0.42	0.0
Dashboard	12	Polycarbonate	1200	2.7	1502	10.0	0.82	0.18	0.0
Seats	7.7	Leather	481	0.135	860	15.0	0.58	0.42	0.0
Human body	10	–	1100	0.432	4200	20.0	0.80	0.20	0.0
Fluid	–	Air	1.225	0.0242	1006.43	–	–	–	–

comprehensively and scientifically. Equivalent temperature, which was proposed by Wyon,[28] and PMV-PPD, which was put forward by Fanger,[29] are the two main objective evaluation methods. However, due to the small space and the many heat sources of the cabin, the gradients of temperature and speed change in different areas of the cabin are larger. Therefore, using PMV-PPD to evaluate the thermal comfort in the cabin will have a larger error. The equivalent temperature, which can effectively reflect the various parts of the body's thermal comfort level, was used in this study. Based on the equivalent temperature theory, the human body model is divided into 16 segments. Figure 10 shows the thermal comfort range of each body segment in summer, as recommended by SAE J2234.

The equivalent temperature of the segment i:

$$T_{\mathrm{eq},i} = T_{s,i} - \frac{8.3 v_{\mathrm{air},i}^{0.6} \cdot S_i \cdot (T_{s,i} - T_{a,i})}{h_{\mathrm{cal},i} \cdot S_i} + \frac{\sum \sigma \cdot \varepsilon_i \cdot f_{i,n} \cdot S_i \cdot \left(T_{s,i}^4 - T_n^4\right) + Q_{\mathrm{sol}}}{h_{\mathrm{cal},i} \cdot S_i} \quad (2)$$

where $T_{s,i}$ represents the surface temperature of the segment, $T_{a,i}$ represents the air temperature around the segment, $v_{\mathrm{air},i}$ is the air velocity around the segment, Q_{sol} represents the body's solar radiation, ε_i is the emissivity, σ is the Stefan constant which equals 5.67×10^{-8} W/(m^2 K^4), $f_{i,\ n}$ represents the effective radiation area coefficient of the segment, $h_{\mathrm{cal},n}$ represents the convection heat transfer coefficient calibrated in a standard environment, and S_i is the surface area of the segment.

The thermal comfort deviation A_{EQT} can describe the overall thermal comfort which is a conversion of the equivalent temperature:

$$A_{\mathrm{EQT}} = \sum_{i=1}^{n} w_i A_i \quad (3)$$

$$A_i = \frac{\frac{1}{2}(T_{\mathrm{max,i}} - T_{\mathrm{min,i}}) - \left|T_{\mathrm{eq},i} - \frac{1}{2}(T_{\mathrm{max,i}} + T_{\mathrm{min,i}})\right|}{\frac{1}{2}(T_{\mathrm{max,i}} - T_{\mathrm{min,i}}) + \left|T_{\mathrm{eq},i} - \frac{1}{2}(T_{\mathrm{max,i}} + T_{\mathrm{min,i}})\right|} = \frac{c-e}{c+e} \times 100\% \quad (4)$$

where ω_i represents the weight of the segment (see Table VII), $T_{\mathrm{eq},i}$ is the equivalent temperature, and $T_{\mathrm{max},i}$ and $T_{\mathrm{min},i}$ respectively, represent the upper and lower limits of the equivalent temperature of the comfort zone.

A_{EQT} represents the deviation between the equivalent temperature of the various segments of the human body and the ideal value of the comfort zone. The value of A_{EQT} is in the range of -1 to 1. When the thermal comfort deviation is less than zero, the overall thermal comfort can be considered uncomfortable. When it is more than zero, the greater the number, the more comfortable the human will feel.

Table VI. Boundary condition

Location	TEC1	TEC2	TEC3	TEC4	TEC5	TEC6
Turbulence intensity	4.6%	4.6%	4.6%	4.6%	4.6%	4.9%
Hydraulic diameter	0.094 m	0.094 m	0.094 m	0.094 m	0.094 m	0.090 m
Inlet temperature	18°C	19°C	19°C	20°C	20°C	21°C
Inlet velocity	3 m/s	3 m/s	3 m/s	3 m/s	3 m/s	2 m/s

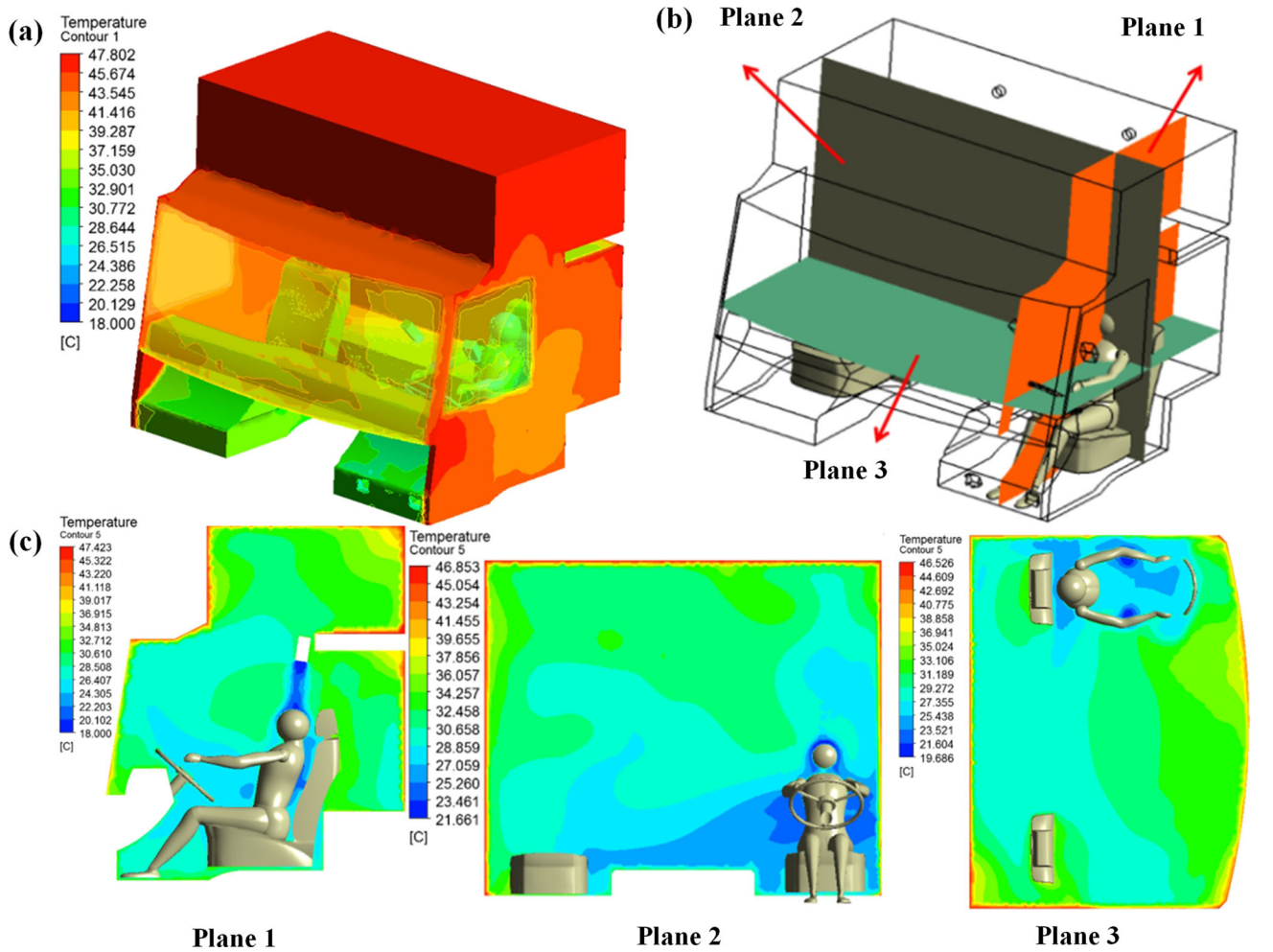

Fig. 8. Temperature maps of the cabin.

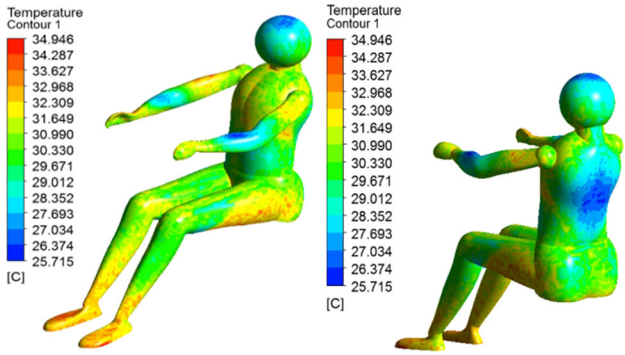

Fig. 9. Temperature maps of the human body.

Figure 11 presents the calculation results of the above working conditions based on equivalent temperature. It can be seen that the head, back and chest equivalent temperatures were close to the ideal value, as were the local thermal comforts of these segments. The feet and left thigh were outside the comfort zone with higher temperatures. The thermal comfort of the upper limbs was generally better than that of the lower limbs. Most body parts were in the comfort interval. The A_{EQT} was 0.235, the cooling effect of the system, can approximately meet the comfort requirements.

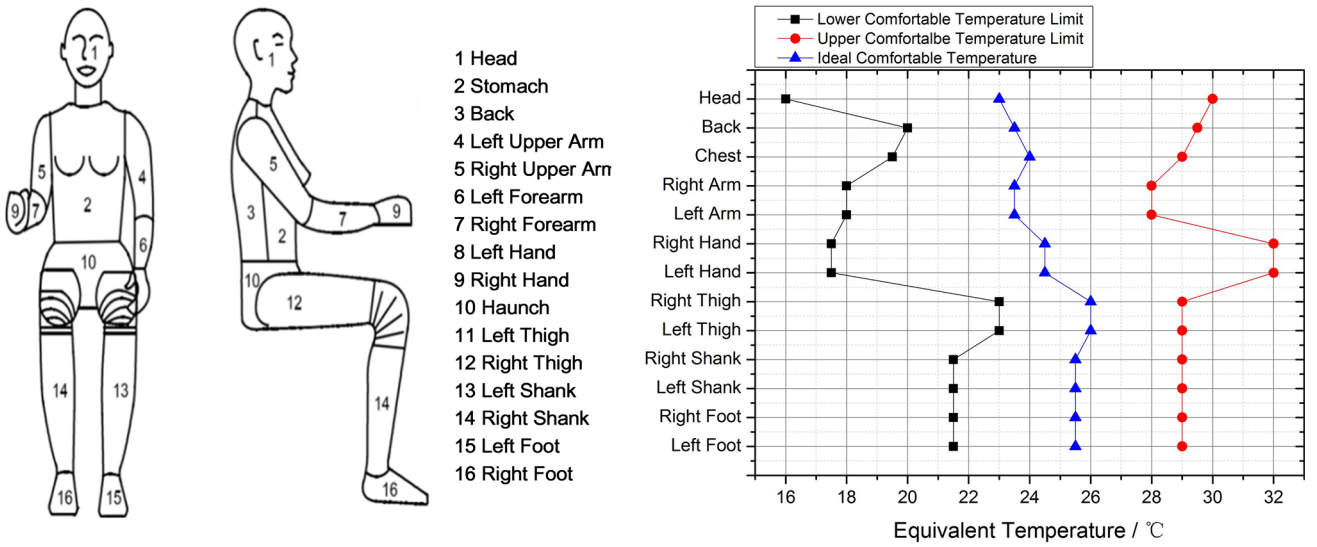

Fig. 10. Thermal comfort range of each body segment.

Table VII. Impact weight of the segment

Segment	Head	Chest	Back	Upper Arm	Forearm	Hand	Thigh	Shank	Foot
Surface area (m^2)	0.18	0.185	0.204	0.077	0.062	0.05	0.16	0.14	0.062
Proportion/ (%)	10.3	10.6	11.7	4	3.5	2.9	9.1	8	3.5
Weight	0.21	0.19	0.19	0.05	0.03	0.01	0.075	0.03	0.01

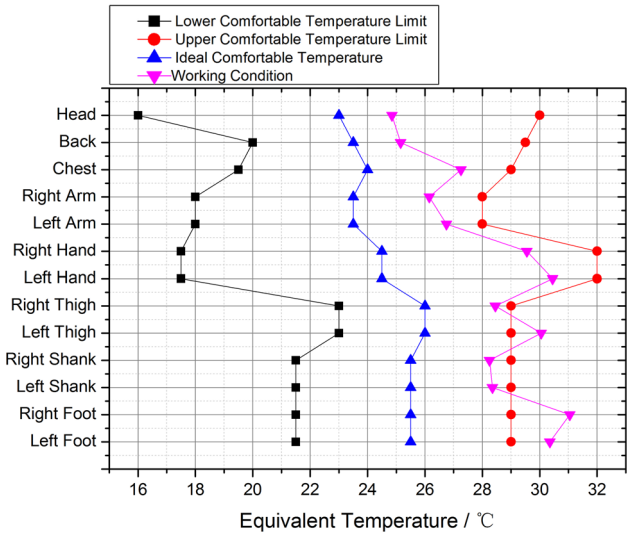

Fig. 11. Equivalent temperature distribution of segments.

CONCLUSION

A localized air conditioning system based on thermoelectric cooling was developed, and a heavy-duty truck cabin was selected for the application. The relationship between the refrigeration performance and the operating current of the TEC devices was studied. The driver's thermal comfort was analyzed based on equivalent temperature and thermal comfort deviation. Under given conditions, most body parts were in the comfort temperature range. The calculation result of the thermal comfort deviation was 0.235. The results indicated that the system can meet the thermal comfort requirements.

ACKNOWLEDGMENTS

This work was supported by the National Natural Science Foundation of China (Grant No. 51805387), the 111 Project (B17034), and the Excellent Dissertation Cultivation Funds of Wuhan University of Technology (Grant No. 2016-YS-049).

REFERENCES

1. S. Chen, N. Li, Y. Hiroshi, and J. Guan, *Energy Build.* 43, 1063 (2011).
2. S. Murshed and N.D. Castro, *Renew. Sust. Energy Rev.* 78, 821 (2017).
3. G. Fraisse, J. Ramousse, D. Sgorlon, and C. Goupil, *Energy Convers. Manag.* 65, 351 (2013).
4. H. Lv, X.D. Wang, T.H. Wang, and C.H. Cheng, *Appl. Energy* 164, 501 (2016).
5. H.L. Tsai and P.T. Le, *Energy Convers. Manag.* 118, 170 (2016).
6. L. Zhu, H. Tan, and J. Yu, *Energy Convers. Manag.* 76, 685 (2013).
7. X. Liu, Y.D. Deng, Z. Li, and C.Q. Su, *Energy Convers. Manag.* 90, 121 (2015).

8. T. Ma, P. Jaideep, E. Srinath, H. Scott, D. Samruddhi, and Q.W. Wang, *Appl. Energy* 185, 1343 (2017).
9. C. Liu, Y.D. Deng, X.Y. Wang, X. Liu, Y.P. Wang, and C.Q. Su, *Appl. Therm. Eng.* 108, 916 (2016).
10. X. Liu, Y.D. Deng, K. Zhang, M. Xu, Y. Xu, and C.Q. Su, *Appl. Therm. Eng.* 71, 364 (2014).
11. Y.P. Wang, S. Li, Y.F. Zhang, X. Yang, Y.D. Deng, and C.Q. Su, *Energy Convers. Manag.* 2016, 266 (2016).
12. R. Shen, X.L. Gou, H.Y. Xu, and K.R. Qiu, *Appl. Energ.* 203, 808 (2017).
13. K. Nicholas and Y.L. Zhang, *Energy Convers. Manag.* 121, 224 (2016).
14. S. Richard, M.A. Wijewardane and Z.J. Yang, *Appl. Therm. Eng.* 112, 1433 (2016).
15. J.L. Niu, L.Z. Zhang, and H.G. Zuo, *Energy Build.* 34, 487–495 (2002).
16. X.Q. Sun, L.F. Zhang, and S.G. Liao, *Appl. Therm. Eng.* 116, 433 (2017).
17. L.M. Shen, H.X. Chen, F. Xiao, Y.X. Yang, and S.W. Wang, *Energy Convers. Manag.* 80, 39 (2014).
18. S.A. Abdul-Wahab, E. Ali, and A.D.M. Ali, et al., *Renew. Energy* 34, 30 (2009).
19. M. Gao and D.M. Rowe, *Appl. Energy* 83, 133 (2006).
20. G. Mark, L.B. Jiang, and R. Saffa, *Int. J. Energy Res.* 34, 776 (2010).
21. Y.M. Zeki, *Energy Build.* 113, 51 (2016).
22. D.L. Zhao and G. Tan, *Appl. Therm. Eng.* 66, 15 (2014).
23. K. Chunkyu, C.W. Lee, F. Lee, K. Jungho and Y. Shin, *SAE 2012 World Congress and Exhibition* (2012).
24. Á.G. Miranda, T.S. Chen, and C.W. Hong, *Energy* 59, 633 (2013).
25. G. Debashis, M.Y. Wang, W. Edward, K.H. Chen, K. Shailendra, and T.Y. Han, *SAE International Journal of Passenger Cars- Mechanical Systems* 5, 885 (2012).
26. K.H. Chen, B. Jeffrey, M.Y. Wang M, G. Debashis, W. Edward, and C. Sourav, *SAE 2015 World Congress and Exhibition* (2015).
27. M.S. Raut and D.P.V. Walke, *Int. J. Eng. Sci. Technol.* 4, 2381 (2012).
28. R.C. Allen, D.P. Scott, J.S. Tony, and A.H. Mark, *SAE Int. J. Aerosp.* 2, 263 (2009).
29. M.S. Jang, C.D. Koh, and I.S. Moon, *Build. Environ.* 42, 55 (2007).